Available online at www.sciencedirect.com
SCIENCE DIRECT®
Journal of Nuclear Materials 328 (2004) 232–242
journal of nuclear materials
www.elsevier.com/locate/jnucmat

Dynamic strain aging under tensile and LCF loading conditions, and their comparison in cold worked 316L stainless steel

Seong-Gu Hong, Soon-Bok Lee *

Department of Mechanical Engineering, Korea Advanced Institute of Science and Technology, 373-1 Guseong-dong, Yuseong-gu, Daejeon 305-701, Republic of Korea

Received 9 July 2003; accepted 13 April 2004

Abstract

Tensile and low-cycle fatigue (LCF) tests were carried out in a wide temperature range from 20 to 750 °C at strain rates of 1×10^{-4}–1×10^{-2}/s for 17% cold worked 316L stainless steel to investigate the conditions for the occurrence of dynamic strain aging (DSA) and its effects on material properties during tensile and LCF deformations. DSA introduced anomalous changes of tensile and LCF properties, and the DSA regimes under tensile and LCF loading conditions coincided with each other. During tensile deformation, DSA can be manifested in the forms of the plateau in the variation of strength with temperature, the minima in the variation of ductility with temperature, the serrated yielding in the stress–strain curves, and the negative strain rate sensitivity (SRS). As for LCF deformation, it can be manifested in the forms of the plateau or the peak in the variation of cyclic peak stress with temperature, the negative temperature dependence of plastic strain amplitude or softening ratio, the negative SRS, and the negative strain rate dependence of plastic strain amplitude or softening ratio.

1. Introduction

Type 316L stainless steel, which has been favored as a structural material in several high-temperature components such as in the primary side of liquid metal cooled fast breeder reactor (LMFBR), stands as a prominent material for the next generation power facilities because of a good combination of its excellent high-temperature tensile and creep strength, corrosion resistance, and enhanced resistance to sensitization and associated intergranular cracking. In LMFBR applications, the components are exposed to severe conditions, such as high temperature, ranging from 300 to 600 °C and undergo temperature-gradient induced cyclic thermal stresses as a result of start-ups and shut-downs. Low-cycle fatigue (LCF) represents a predominant failure mode; thus specific attention on LCF is needed in the design and life assessment of such components. In austenitic stainless steels [1–4], the reduction of the fatigue resistance with increasing the temperature has been reported, and it was ascribed to the change of the cyclic plastic deformation mechanism, creep, and oxidation effects or interactions among these factors. It has also been noticed that in the temperature range of 300–600 °C, dynamic strain aging (DSA) induces a significant change in material properties, such as strength and ductility, and, thus, more detailed research for the influence of DSA on LCF behavior is required in this temperature region.

The importance of DSA effect on material behavior has been reported in several types of materials [1–6].

* Corresponding author. Tel.: +82-42 869 3029; fax: +82-42 869 3210.
E-mail address: sblee@kaist.ac.kr (S.-B. Lee).

0022-3115/$ - see front matter © 2004 Elsevier B.V. All rights reserved.
doi:10.1016/j.jnucmat.2004.04.331

Dynamic strain aging is the phenomenon of interactions between diffusing solute atoms and mobile dislocations during plastic deformation and depends on the deformation rate and temperature, which govern the velocities of mobile dislocations and diffusing solute atoms, respectively. At present, some research has been conducted on DSA, and it is well established for monotonic tensile loading conditions. However, few systematic investigations have been reported about the influence of DSA on LCF behavior. During fatigue deformation, the testing time is prolonged and the developed microstructure differs from that during monotonic tensile deformation, and, thus, these factors will affect DSA. Tsuzaki et al. [7] reported that the temperature range required for DSA depends on the deformation mode in a type 304 austenitic stainless steel; at a given strain rate, the lower critical temperature for the appearance of DSA during strain-controlled fatigue deformation is much lower than that during monotonic tensile deformation. They proposed a model in which the above result is shown to be caused by the difference between the temporary arrest times of moving dislocations, during which the dislocations are locked by solute atoms. They also proposed that the arrest time for fatigue loading is longer because of the shuttling motion of dislocations. However, in their study [7], only a serrated flow was used to determine the DSA regime. According to the references [8,9], the domain of DSA is generally broader than that of the serrated yielding, and includes it. Hence, determining the DSA regime while using it should be done with caution.

While serrated yielding is the most commonly observed manifestation of DSA, there are various other concurrent phenomena. Other anomalies associated with DSA have been described by Rodriguez [10]; during monotonic tensile deformation, DSA is manifested by the serrated flow in the stress–strain curve, the peak or the plateau in the variation of material strength with temperature, the minima in the variation of ductility with temperature, and the negative strain-rate sensitivity (SRS). In case of fatigue deformation, besides the above manifestations, the negative temperature dependence of the plastic strain amplitude or softening ratio (the amount of cyclic softening during fatigue deformation) and the negative strain-rate dependence of the plastic strain amplitude or softening ratio have been noticed as the evidence of DSA [11,12]. Therefore, using these several manifestations of DSA, the conditions of the occurrence of DSA can be determined at each deformation mode.

In this study, tensile and LCF tests were carried out in a wide temperature range, from 20 to 750 °C, and strain rates of 1×10^{-4}–1×10^{-2}/s for the 17% cold-worked (CW) 316L stainless steel to elucidate the conditions for the occurrence of DSA and its effects on material properties during tensile and LCF deformations.

2. Experimental procedure

2.1. Material and specimen

The material used in this study was 17% CW 316L stainless steel having the following chemical composition in wt%: C – 0.025, Si – 0.41, Mn – 1.41, P – 0.025, S – 0.025, Ni – 10.22, Cr – 16.16, Mo – 2.09, N – 0.043, Fe–balance. The as-received material was manufactured by the following processes: the material was solution-treated at 1100 °C for 40 min, then water-quenched, and, finally, a round bar with a diameter of 16 mm was made through the cold-drawn process, which introduced 17% tensile pre-strain. This treatment yielded an average intercept grain size of 44.2 μm. The as-received material was fabricated into dog-bone type specimens with a gauge length of 36 mm and a gauge diameter of 8 mm in accordance with ASTM standard E606-92. The specimen surface was polished along the longitudinal direction with emery paper down to #2000 (≈13 m) in order to remove surface defects, such as machining marks and scratches.

2.2. Test equipment and procedure

A closed-loop servo-hydraulic test system with 5 ton capacity manufactured by MTS was used to accomplish tensile and LCF tests, and a three-zone resistance type furnace that can control temperature within a variation of ± 1 °C at steady-state was used for temperature control. A high temperature extensometer (MTS model no.: 632-13F-20, gauge length: 25 mm) was used to measure a strain and control a strain signal.

Tensile tests were conducted in air by maintaining constant cross-head speeds of 0.2, 2, and 20 mm/min. in the temperature region from 20 to 750 °C. Cross-head speeds of 0.2, 2, and 20 mm/min. correspond to strain rates of 1×10^{-4}, 1×10^{-3}, and 1×10^{-2}/s, respectively. LCF tests were carried out in air under a fully reversed total axial strain control mode employing a triangular waveform at room temperature (RT), 200, 400, 550, 600, and 650 °C. A strain amplitude of 0.5% was employed for all LCF tests, and the employed strain rates were 1×10^{-4}, 1×10^{-3}, and 1×10^{-2}/s.

2.3. Metallography

The fracture surfaces of tensile failed specimens were examined by SX-30E scanning electron microscope and the changes of the dislocation structure after LCF testing were studied by JEOL 2000FX transmission electron microscope (TEM). Samples for TEM were obtained from thin slices cut at a distance of 1mm away from the fracture surface and then electropolished in a solution containing 5% perchloric acid and 95% acetic acid at 70 V and 10 °C.

3. Results and discussion

3.1. Tensile test

3.1.1. Serrated yielding

Serrated yielding is defined as the repeated and systematic fluctuations of the load, i.e., load drops in the stress–strain curves during tensile deformation. In austenitic stainless steels, the most widely accepted mechanism of serrated yielding is dynamic strain aging during plastic deformation as a result of the interaction between solute atoms and mobile dislocations [13]. Mannan et al. [14] have investigated DSA in a 316 stainless steel. At low temperatures below 350 °C, the diffusing velocity of the interstitial solute atoms, such as carbon and nitrogen, is fast enough to move and age the dislocations, and at high temperatures over 400–650 °C, plastic deformation-induced vacancies enhance the diffusion of chromium atoms, causing the aging of the dislocations by the chromium atmospheres.

The conditions of temperature and strain rate for the occurrence of serrated yielding are shown in Fig. 1. Types A, B, D, and E serrations, which are defined in Ref. [10], are observed in the stress–strain curves. At each strain rate, Type D serration occurred alone at low temperatures and Types A, B, E serrations at high temperatures (Fig. 2). Types A and B serrations simultaneously occurred at low strains and change to Type E serration at high strains. As shown in Fig. 1, the regime of serrated yielding depends on temperature and strain rate and is moved to a higher temperature region as the strain rate increases. Serrated yielding occurred in the temperature region from 300 to 550 °C at a strain rate of 1×10^{-4}/s, in 450–650 °C at 1×10^{-3}/s, and in 550–700 °C at 1×10^{-2}/s.

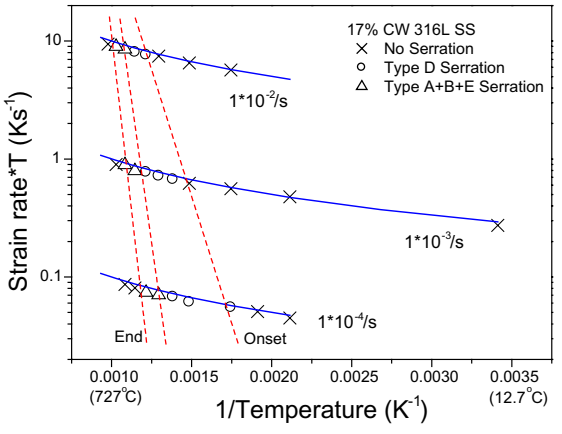

Fig. 1. Regimes of occurrence of serrated yielding in the stress–strain curves.

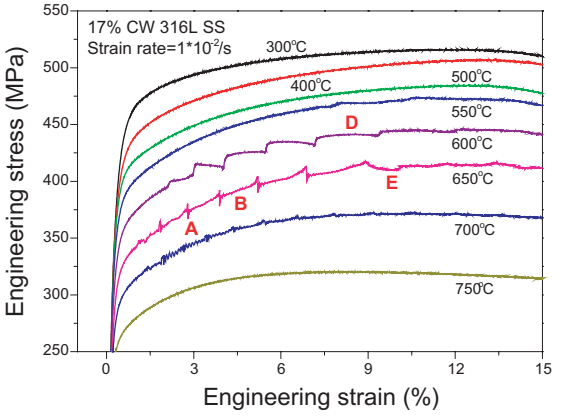

Fig. 2. Segments of the stress–strain curves from tensile tests at $\dot{\varepsilon} = 1 \times 10^{-2}$/s.

3.1.2. Influence of DSA on material strength

The variation of tensile strength with temperature at each strain rate is presented in Fig. 3(a). Material strength decreases with increasing temperature, and there exists a temperature region (250–600 °C) where the reduction of strength with increasing temperature is retarded or even slightly increased. Such anomalous behavior is attributed to the DSA-induced hardening.

As shown in Fig. 3(a), the influence of strain rate on yield strength, which is determined by the 0.2% offset strain method, was negligible but the true ultimate tensile strength (UTS), defined as the '$(1 + e_n)\cdot$(engineering UTS)' where e_n represents an engineering strain at onset of necking, was significantly affected by the strain rate. The strain-rate dependence of the true UTS depends on the temperature and can be characterized by three regions: in Region I below 250 °C, there was no significant effect of strain rate. In Region II over 250–600 °C, the negative strain-rate stress response was observed, which means that strain hardening decreases as the strain rate increases. In Region III above 600 °C, the positive strain-rate stress response was observed, which means that strain hardening increases as the strain rate increases. According to Beukel [15], DSA can be manifested by the negative SRS, which is defined as $d\sigma/d\ln\dot{\varepsilon}$. The SRS values defined as $\Delta\sigma/\Delta\ln\dot{\varepsilon}$ were calculated at each temperature, and the result is presented in Fig. 3(b). The SRS value becomes negative in the temperature range of 250–600 °C, and, thus, this temperature region is considered to be the DSA regime.

3.1.3. Influence of DSA on material ductility

Elongation was measured on the gauge length of 25 mm during tensile tests to investigate the influence of temperature and strain rate on material ductility (Fig. 3(c)). The result reveals that there is a drastic reduction of elongation when the temperature increases from 20 to

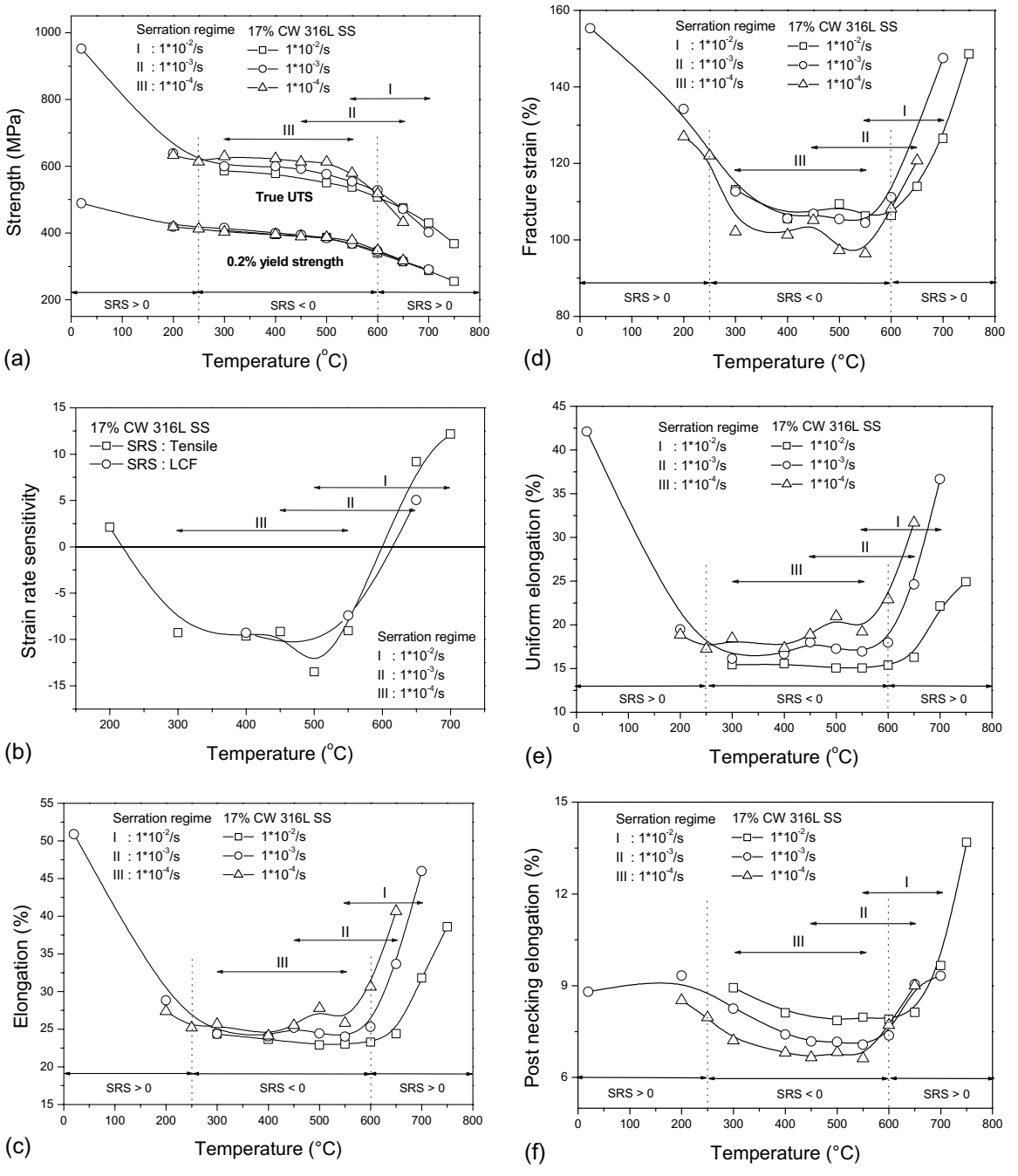

Fig. 3. The variation of tensile properties with temperature and strain rate: (a) strength; (b) strain rate sensitivity; (c) elongation; (d) fracture strain; (e) uniform elongation and (f) post-necking elongation.

200 °C, and the minima in the variation of elongation with temperature are observed in the temperature region from 250 to 600 °C. This minimum region of elongation depends on the strain rate, and moves to a higher temperature as the strain rate increases. The occurrence of the minimum elongation is attributed to the DSA-induced embrittlement. Its strain-rate dependency is consistent with that the DSA regime moves to a higher temperature as the strain rate increases.

In the DSA regime, the DSA effect becomes more pronounced as the strain rate decreases, and, thus, leads to the reduction of ductility. However, as shown in

Fig. 3(c), when the elongation is used as a measure of the material ductility, the opposite result is noted in the temperature region from 250 to 600 °C where DSA operates, which implies that the elongation increased as the strain rate decreased. This result is contrary to the generally known influence of DSA on ductility. Fracture strain, defined as '$\ln(A_i/A_f)$' where A_i and A_f represent the initial area and the area at fracture, respectively, was calculated and the result is presented in Fig. 3(d). At each strain rate, the variation of fracture strain with temperature is similar with that of elongation. However, in the temperature region from 250 to 600 °C, fracture strain decreases with reduced strain rate and beyond 600 °C where DSA does not operate any longer, the fracture strain increases with decreasing the strain rate. These results are well coincident with the influence of DSA on ductility, and therefore, the fracture strain based on the area reduction of the test specimen is thought to be a proper measure of material ductility.

Elongation is defined as the strain at final fracture in the engineering stress–strain curve and can be divided into two values: the uniform elongation (UEL) and the post-necking elongation (PNEL), which represent the engineering strain up to the onset of necking and the engineering strain from onset of necking to final fracture respectively. The variations of UEL and PNEL with temperature at each strain rate are shown in Fig. 3(e) and (f). At each strain rate, UEL and PNEL have the minimum values in the DSA regime (250–600 °C). UEL shows a similar tendency with elongation. At all test temperatures, UEL increased as the strain rate decreased. However, the opposite was observed in PNEL. PNEL decreased with reduced strain rate in the DSA regime but beyond 600 °C (in the non-DSA regime), PNEL increased as the strain rate decreased. The fracture strain will be significantly affected by PNEL since the deformation is localized after necking. This is evidenced from Fig. 3(d) and (f), where the variations of the fracture strain and PNEL with the strain rate coincided with each other. Hence, in the DSA regime, the reduction of ductility (fracture strain) with decreasing strain rate is attributed to the reduction of PNEL. The DSA-induced reduction of PNEL can be evidenced by examining the fracture surface of the tensile tested specimen. The necking produces a triaxial stress state in the center of the specimen, which promotes void nucleation and growth in the larger particles. Upon further strain, the voids coalesce, resulting in a fibrous zone (a penny-shaped flaw). This fibrous zone size is related to PNEL. According to the previous research [11], the tensile fracture mechanism changed from the classic 'cup and cone' type fracture in the non-DSA regime to the

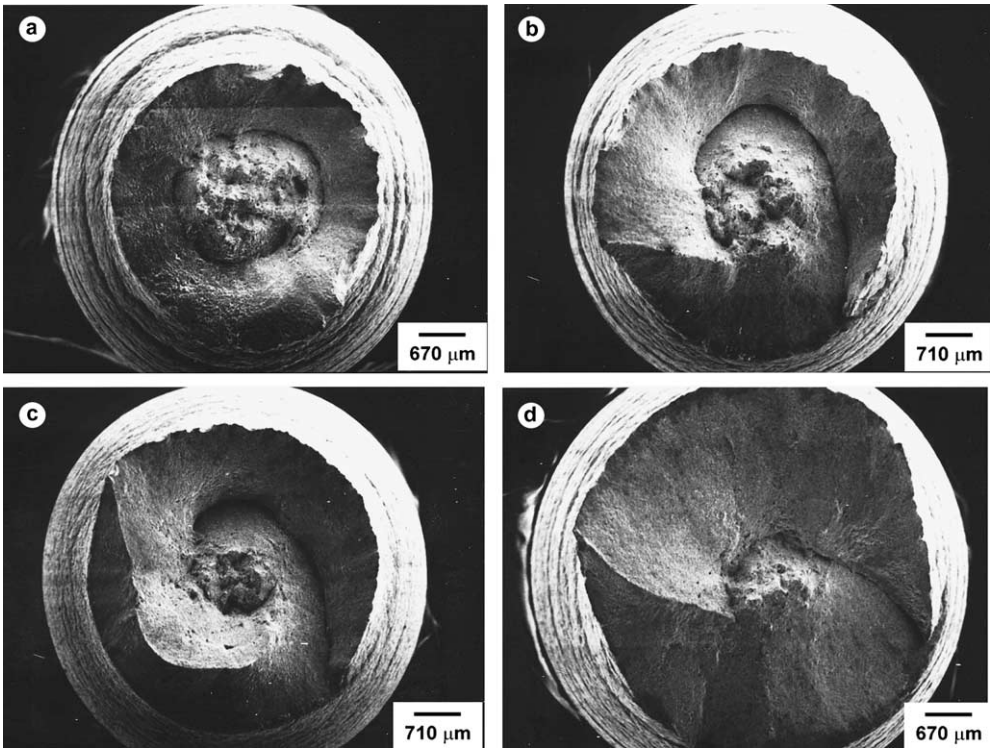

Fig. 4. SEM micrographs of tensile fractured specimens: (a) 200 °C, $\dot{\varepsilon} = 1 \times 10^{-4}$/s; (b) 550 °C, $\dot{\varepsilon} = 1 \times 10^{-2}$/s; (c) 550 °C, $\dot{\varepsilon} = 1 \times 10^{-3}$/s and (d) 550 °C, $\dot{\varepsilon} = 1 \times 10^{-4}$/s.

'cup and cone' fracture in the DSA regime that has a reduced and twisted fibrous zone, compared to that in the non-DSA regime, as shown in Fig. 4. From Fig. 4(b)–(d), it is also observed that the enhanced DSA effect due to the reduced strain rate introduces the reduction of the fibrous zone size, and this fact coincides with the reduction of PNEL as the strain rate decreases.

3.1.4. Dynamic strain aging under tensile loading

Based on the several manifestations mentioned in the above sections, the DSA regime during tensile deformation can be summarized as follows: The DSA regimes manifested by the plateau in the variation of strength with temperature, the minima in the variation of ductility with temperature, and the negative SRS coincided well with each other, and moved to a higher temperature region as the strain rate increased. DSA occurred in the temperature region from 250 to 550 °C at a strain rate of 1×10^{-4}/s, in 250–600 °C at 1×10^{-3}/s, and 250–650 °C at 1×10^{-2}/s. However, it shows some difference with the regime of serrated yielding. At high strain rates of 1×10^{-3}–1×10^{-2}/s, although serrated yielding does not appear in the stress–strain curves in the temperature range from 250 to 400 °C, other manifestations of DSA such as the plateau in the variation of strength with temperature, the minima in the variation of ductility with temperature, and the negative SRS were observed. This result clearly indicates that DSA commences earlier than is manifested in the form of serrated yielding. The highest temperature for DSA was 700 °C at 1×10^{-2}/s and manifested by serrated yielding.

3.2. Low-cycle fatigue test

3.2.1. Cyclic stress response

Cyclic softening behaviors were observed through a whole life except the initial few cycles at all test conditions (Fig. 5(a)), and it is attributed to the 17% tensile prestrain that has been introduced in the as-received material by cold-working in the manufacturing process. According to the references [16–18], cyclic softening has been reported in the materials that are manufactured by the cold work process or have a high initial dislocation density. Cyclic softening of cold-worked materials occurs when the annihilation rate of the dislocations is greater than their generation rate, causing a net decrease in the dislocation density, or when the rearrangement of previously formed dislocation structure takes place with a number of cycles (dynamic recovery), resulting in an increase in the mean free path of dislocations [16,18]. When the rearrangement of the previously formed dislocation structure has completed, the cyclic behavior of material becomes stable.

As shown in Fig. 5(a), cyclic stress responses at all test conditions can be characterized by three stages: in stage I, cyclic hardening is observed and the peak stress

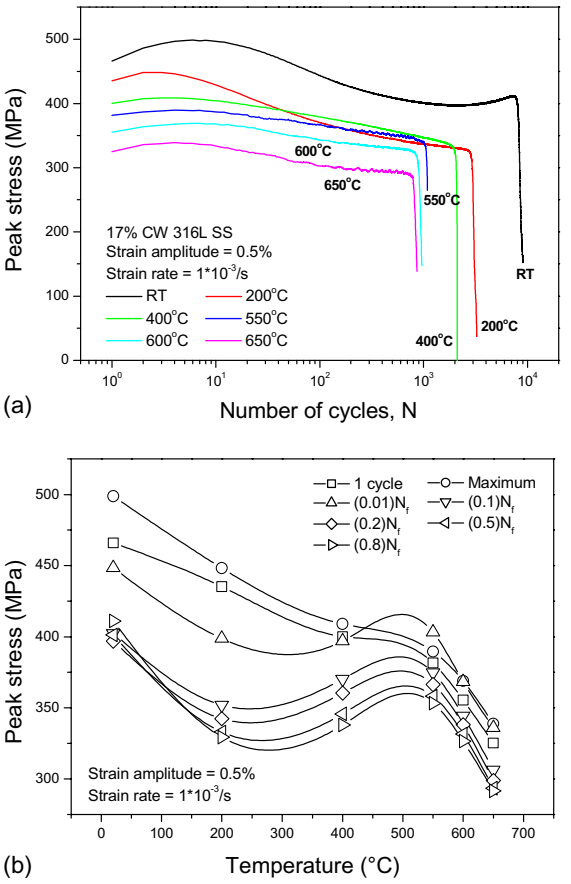

Fig. 5. Influence of temperature on cyclic stress responses at $\Delta\varepsilon_t = \pm0.5\%$: (a) peak stress vs. number of cycles and (b) peak stress vs. temperature.

reaches a maximum value after the initial few cycles. In stage II (about 90% of the fatigue life), cyclic softening occurs and continues to the macrocrack-initiation point where the steep decrement in the peak stress is developed. In stage III, the steep reduction in the peak stress is introduced since the effective load-bearing area is reduced due to the propagation of macrocracks. The static recovery, which is introduced during the thermal stabilizing process of a specimen before tests, is thought to be the reason for the occurrence of cyclic hardening in stage I.

3.2.2. Influence of temperature on LCF properties

The evolution of the cyclic peak stress with a number of cycles is depicted in Fig. 5. During the initial few cycles, which correspond to the peak stress at the first cycle and the maximum peak stress in Fig. 5(b), an increased temperature introduced a decrease in the cyclic peak stress and the retardation in the reduction of the peak stress with increasing temperature was noted in the

temperature region from 450 to 550 °C. This result indicates that DSA operates in the temperature range of 450–550 °C. With an increasing number of cycles, anomalous cyclic behavior characterized by the higher peak stress or retardation in the reduction of the peak stress with increasing temperature was more pronounced and extended to the temperature region from 250 to 600 °C, indicating that the domain of the occurrence of DSA extended and the DSA effect became more pronounced with a number of cycles. After 1% of fatigue life ($N/N_f = 0.01$), the temperature dependence of the cyclic peak stresses does not change with the number of cycles, and the temperature region that shows the most pronounced DSA effect was in the range of 450–550 °C. Such a negative temperature dependence of the cyclic peak stress is thought to come from the DSA-induced hardening. In the temperature region from 250 to 600 °C, DSA operates during LCF deformation, causing a decrease in the amount of cyclic softening, and, thus, leads to a higher cyclic peak stress. However, in the non-DSA regime, the opposite resulted since the DSA-induced hardening effect is removed.

The dislocation structure of austenitic stainless steels involving 316L(N) stainless steel changes from a cell structure at temperatures below 300 °C to a planar one between 300 and 600 °C (DSA regime) and back to a cell or subgrain structure beyond 600 °C [1–4]. As shown in Fig. 6, similar results were obtained in this study: a

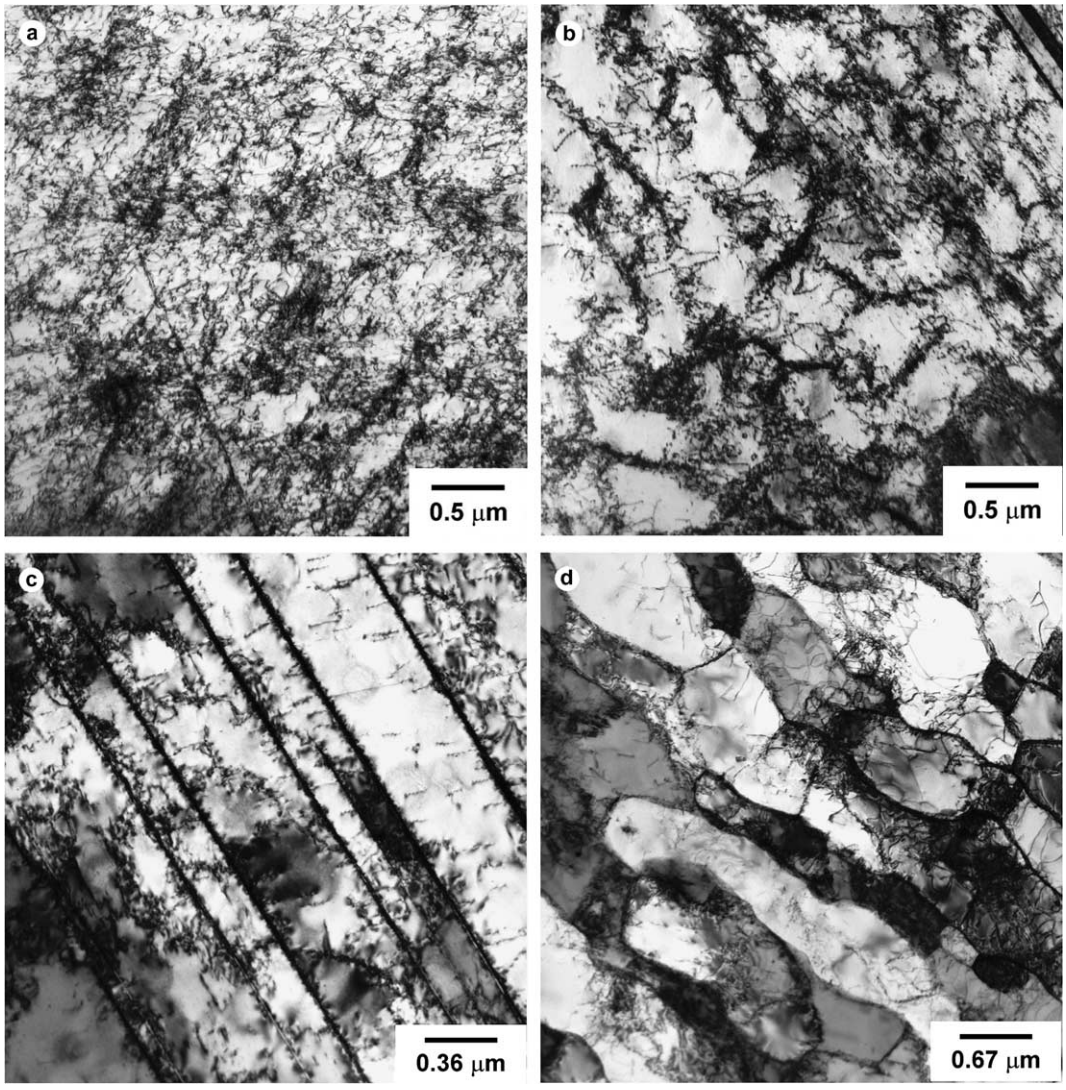

Fig. 6. TEM micrographs depicting the substructure: (a) as-received material; (b) RT, $\Delta\varepsilon_t = \pm 0.5\%$; $\dot{\varepsilon} = 1 \times 10^{-3}$/s; (c) 400 °C, $\Delta\varepsilon_t = \pm 0.5\%$, $\dot{\varepsilon} = 1 \times 10^{-4}$/s and (d) 650 °C, $\Delta\varepsilon t = \pm 0.5\%$, $\dot{\varepsilon} = 3.2 \times 10^{-5}$/s.

cellular dislocation structure below 250 °C and at about 600 °C, a planar band structure with a high dislocation density at intermediate temperatures where DSA operates, and a subgrain structure above 650 °C with low strain rates. In the regime of DSA, the mechanism of interaction occurs between the mobile dislocations and the solute atmosphere restricting the cross slip of dislocations and increasing the slip planarity, which causes an increase in flow stress needed to impose the same total strain (DSA-induced hardening), and, thus, a decrease in the amount of cyclic softening.

The positive temperature dependence of the cyclic peak stress during the initial few cycles appears to result from the effect of the initial dislocation structure formed by prior cold work, and this effect is weakened and disappears with a number of cycles due to the rearrangement of the initial dislocation structure.

As mentioned above, the cyclic-softening behavior strongly depends on the temperature and strain rate. To quantify the amount of cyclic softening during LCF deformation and to elucidate its temperature and strain rate dependency in detail, the parameter 'softening ratio' defined as Eq. (1) is introduced.

$$\text{Softening ratio} = \frac{\sigma_{\max} - \sigma_{\max}|_{N_f/2}}{\sigma_{\max}}, \tag{1}$$

where $\sigma_{\max}$ and $\sigma_{\max}|_{N_f/2}$ represent a maximum peak stress and a peak stress at half-life, respectively. The variation of softening ratio with temperature at each strain rate is shown in Fig. 7(a). The DSA-induced hardening introduced a negative temperature dependence of the softening ratio (that is, a decrease in the softening ratio with increasing the temperature), and the DSA regime was in the temperature region from 400 to 550 °C at a strain rate of 1×10^{-4}/s, in 200–600 °C at 1×10^{-3}/s, and in 400–650 °C at 1×10^{-2}/s. In case of strain rates of 1×10^{-4} and 1×10^{-2}/s, LCF tests were carried out only in the temperature region from 400 to 650 °C, and, thus, an analysis for temperatures below 400 °C cannot be given.

According to Ref. [12], a negative temperature dependence of the plastic strain amplitude at half-life (that is, a decrease in the half-life plastic strain amplitude with increasing temperature) has been noticed in the DSA regime in LCF. Such a negative temperature dependence of the plastic strain amplitude results from the plastic strain amplitude being calculated from the difference between the total strain amplitude and elastic strain amplitude. In the DSA regime, material is hardened by DSA, causing an increase in the flow stress needed to impose the same total strain, and, thus, leading to an increase in the elastic strain amplitude. The variation of the plastic strain amplitude at half-life with temperature is depicted in Fig. 7(b), and the results reveal that a negative temperature dependence of the plastic strain amplitude occurred in the temperature region from 200 to 550 °C.

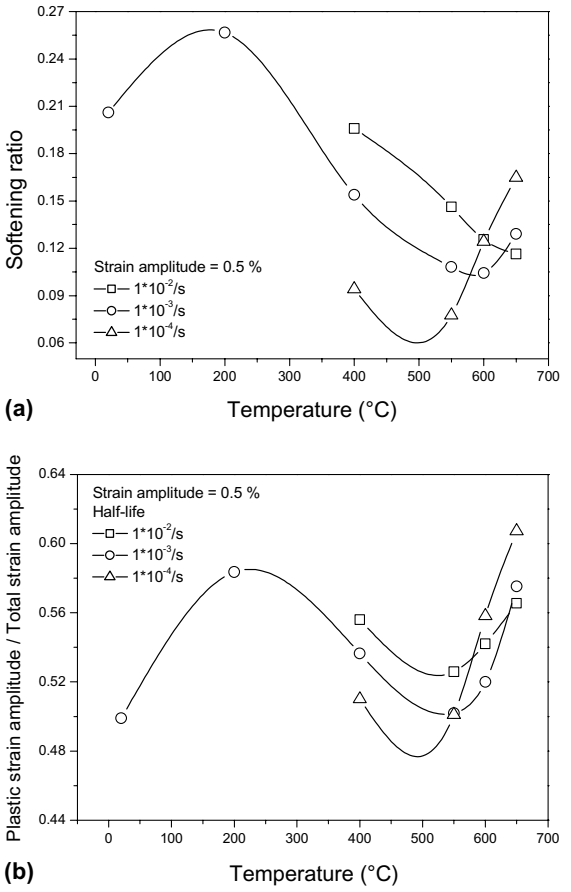

Fig. 7. Influence of temperature on LCF properties at $\Delta\varepsilon_t = \pm0.5\%$: (a) softening ratio and (b) plastic strain amplitude.

3.2.3. Influence of strain rate on LCF properties

As shown in Fig. 8, the influence of the strain rate on cyclic stress responses depended on temperature and could be characterized by 2 regions. A negative strain-rate–stress response in 400–550 °C, transition at 600 °C, and a positive strain-rate stress response at 650 °C were observed. When the regime of the negative strain-rate stress response is analyzed in detail, it is in the temperature range of 400–550 °C at strain rates of 1×10^{-4}–1×10^{-2}/s and in 600 °C at 1×10^{-3}–1×10^{-2}/s. The variation of peak stresses at half-life with strain rate at each temperature is presented in Fig. 9(a), and the result reflects well the anomalous behavior in 400–600 °C characterized by a negative strain rate stress response. SRS values in LCF were calculated at each temperature using the relation between the peak stress at half-life and strain rate, and the results are compared with that in the tensile loading

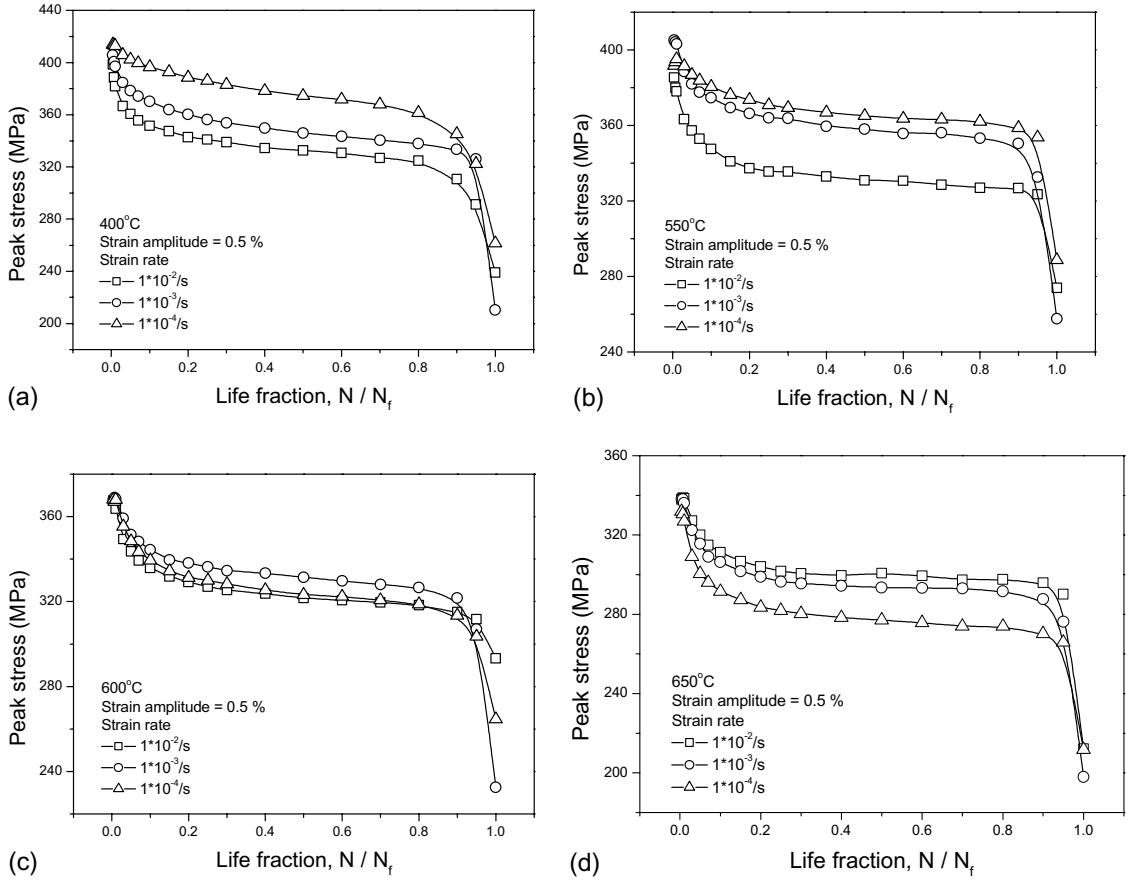

Fig. 8. Influence of strain rate on cyclic stress responses at $\Delta\varepsilon_t = \pm 0.5\%$: (a) 400 °C; (b) 550 °C; (c) 600 °C and (d) 650 °C.

condition (Fig. 3(b)). The negative SRS regimes (the DSA regimes) between tensile and LCF loading conditions coincide with each other in the temperature region from 400 to 600 °C, and SRS values under two loading conditions are similar. It is noticed that SRS at each temperature in LCF is maintained at a constant value from 10% of fatigue life ($N/N_f = 0.1$) to the initiation of stage III ($N/N_f = 0.9$) at all temperatures, as shown in Fig. 10. This result indicates that if the material is stabilized, SRS would be maintained at a constant value.

The negative strain rate stress response in the DSA regime appears to result from an increase in the total dislocation density during deformation. According to reference [4], an increase in the dislocation density with decreasing the strain rate has been reported in the DSA regime for 316L(N) stainless steel. During DSA, slow moving dislocations become easily aged by the solute atmosphere, and, thus, additional dislocations are generated to maintain the imposed deformation rate. This mechanism causes an increase in the total dislocation density. The matrix is hardened due to an increase in the dislocation density, causing an increase in the flow stress needed to impose the same total strain during successive cycles.

In the DSA regime, the dynamic strain aging effect will become more pronounced as strain rate decreases; An enhanced DSA effect of this type with reduced strain rate was manifested in the form of the negative strain rate dependences of half-life plastic strain amplitude or softening ratio in the temperature region from 400 to 600 °C at strain rates of 1×10^{-4}–1×10^{-2}/s, in case of 600 °C at 1×10^{-3}–1×10^{-2}/s (Fig. 9(b) and (c)). However, in the non-DSA regime above 600 °C, the opposite was observed since the DSA effect is removed and thermally assisted recovery effect is enhanced with decreasing strain rate.

3.2.4. Dynamic strain aging under low-cycle fatigue loading

Dynamic strain aging under LCF loading can be manifested in the forms of the plateau or the peak in the variation of cyclic peak stress with temperature, the

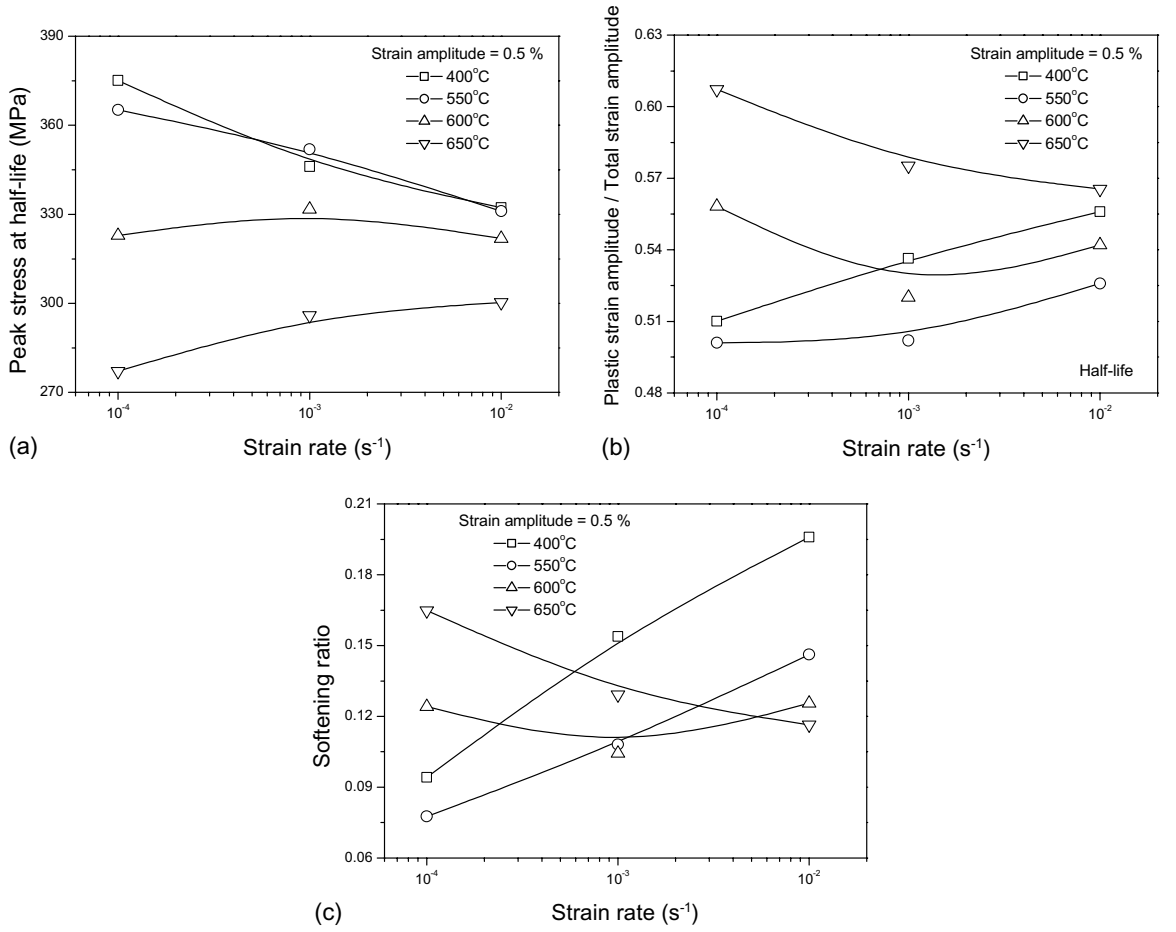

Fig. 9. Influence of strain rate on LCF properties at $\Delta\varepsilon_t = \pm 0.5\%$: (a) peak stress; (b) plastic strain amplitude and (c) softening ratio.

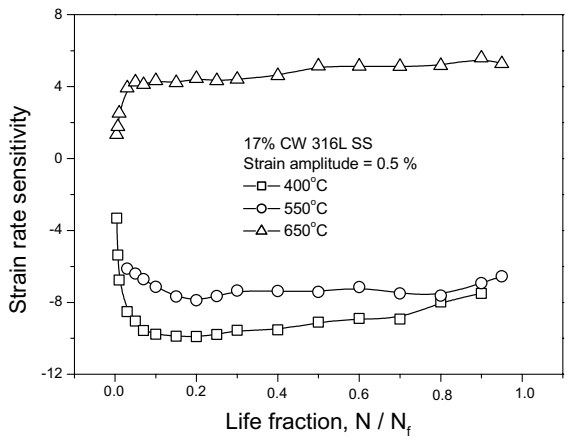

Fig. 10. Evolution of the strain rate sensitivity with number of cycles during LCF deformation at $\Delta\varepsilon_t = \pm 0.5\%$.

negative temperature dependence of plastic strain amplitude or softening ratio, the negative SRS, and the negative strain rate dependence of plastic strain amplitude or softening ratio. Based on the results, the regime of DSA in LCF was in the temperature range of 250–550 °C at a strain rate of 1×10^{-4}/s, in 250–600 °C at 1×10^{-3}/s, and in 250–650 °C at 1×10^{-2}/s, and was consistent with that in the tensile loading condition.

In the present study, serrated yielding was not observed in the stress–strain hysteresis loops during LCF deformation. This absence is thought to result from the total strain amplitude of 0.5% used in LCF tests being too small compared with the critical strain that is needed for serrated yielding to occur. In case of tensile deformation, serrated yielding occurred at a strain above 1%.

4. Conclusions

Dynamic strain aging introduced anomalous changes of tensile and LCF properties of 17% CW 316L stainless

steel and, based on the results, the following conclusions were made:

(1) During tensile deformation, the regimes of DSA manifested by the plateau in the variation of strength with temperature, the minima in the variation of ductility with temperature, and the negative SRS coincided well with each other, and moved to a higher temperature region as strain rate increased. However, some difference was shown with the regime of occurrence of the serrated yielding in the stress–strain curves.
(2) Although serrated yielding does not appear in the stress–strain curves in the temperature range of 250–400 °C at the high strain rates of 1×10^{-3}–1×10^{-2}/s, other manifestations of DSA were observed, such as the plateau in the variation of strength with temperature, the minima in the variation of ductility with temperature, and the negative SRS. This indicates that DSA commences earlier than is manifested in the form of the serrated yielding.
(3) The DSA-induced embrittlement is thought to come from the change of the fracture mechanism. DSA introduced the reduction of the fibrous zone and it was well consistent with the reduction of the post-necking elongation in the DSA regime.
(4) Cyclic stress response depended on temperature and strain rate, and DSA-induced hardening reduced the softening ratio (the amount of cyclic softening during LCF deformation) in 250–600 °C.
(5) During LCF deformation, DSA can be manifested in the forms of the plateau or the peak in the variation of cyclic peak stress with temperature, the negative temperature dependence of plastic strain amplitude or softening ratio, the negative SRS, and the negative strain rate dependence of plastic strain amplitude or softening ratio.
(6) The DSA regimes between tensile and LCF loading conditions coincided with each other, and were in the temperature region from 250 to 550 °C at a strain rate of 1×10^{-4}/s, in 250–600 °C at 1×10^{-3}/s, and in 250–650 °C at 1×10^{-2}/s.

Acknowledgements

This work has been supported by Computer Aided Reliability Evaluation (CARE) National Research Laboratory in Korea Advanced Institute of Science and Technology (KAIST).

References

[1] K. Kanazawa, K. Yamaguchi, S. Nishijima, in: Solomon H.D., G.R. Halford, L.R. Kaisand, B.N. Leis (Eds.), Low Cycle Fatigue, ASTM STP, 942, American Society for Testing and Materials, Philadelphia, 1988, p. 519.
[2] J. Bressers, in: Proceedings of International Conference on High Temperature Alloys and Their Exploitable Potential, Elsevier Applied Science, Amsterdam, 1987, p. 385.
[3] M. Valsan, D.H. Sastry, K. Bhanu Sankara Rao, S.L. Mannan, Metall. Trans. 25A (1995) 159.
[4] V.S. Srinivasan, M. Valsan, R. Sandhya, K. Bhanu Sankara Rao, S.L. Mannan, D.H. Sastry, Int. J. Fatigue 21 (1999) 11.
[5] J.M. Robinson, M.P. Shaw, Int. Mater. Rev. 39 (3) (1994) 113.
[6] L.J. Chen, P.K. Liaw, H. Wang, Y.H. He, R.L. McDaniels, L. Jiang, B. Yang, D.L. Klarstrom, Mech. Mater. 36 (2004) 85.
[7] K. Tsuzaki, T. Hori, T. Maki, I. Tamura, Mater. Sci. Eng. A 61 (1983) 247.
[8] R.A. Mulford, U.F. Kocks, Acta Metall. 27 (1979) 1125.
[9] E. Pink, J. Krol, Mater. Sci. Eng. A 75 (1985) 87.
[10] P. Rodriguez, in: Encyclopedia of Materials Science and Engineering, Suppl. vol. 1, Pergamon, New York, 1988, p. 504.
[11] S.G. Hong, S.B. Lee, Int. J. Fatigue 26 (8) (2004) 889.
[12] K. Bhanu Sankara Rao, M. Valsan, R. Sandhya, S.L. Mannan, P. Rodriguez, High Temp. Mater. Proc. 7 (1986) 171.
[13] P. Rodriguez, Bull. Mater. Sci. 6 (1984) 653.
[14] S.L. Mannan, K.G. Samuel, P. Rodriguez, Trans. Ind. Inst. Metals 36 (1983) 313.
[15] A. van den Beukel, Acta Metall. 28 (1980) 965.
[16] K. Bhanu Sankara Rao, M. Valsan, R. Sandhya, S.L. Mannan, P. Rodriguez, Metall. Trans. 24A (1993) 913.
[17] W.J. Plumbridge, M.E. Dalski, P.J. Castle, Fract. Eng. Mater. Struct. 3 (1980) 177.
[18] S. Ganesh Sundara Raman, K.A. Padmanabhan, Int. J. Fatigue 18 (2) (1996) 71.